A framework for dynamic risk assessment with condition monitoring data and inspection data

Jinduo Xing [1], Zhiguo Zeng [1], Enrico Zio [1,2,3]

[1] Chair System Science and the Energy Challenge, Fondation Electricité de France (EDF), CentraleSupélec, Université Paris Saclay, Gif-sur-Yvette, France

[2] Energy Department, Politecnico di Milano, Milan, Italy

[3] Department of Nuclear Engineering, College of Engineering, Kyung Hee University, Republic of Korea

jinduo.xing@centralesupelec.fr, zhiguo.zeng@centralesupelec.fr, enrico.zio@ecp.fr

Abstract

In this paper, a framework is proposed for integrating condition monitoring and inspection data in Dynamic Risk Assessment (DRA). Condition monitoring data are online-collected by sensors and indirectly relate to component degradation; inspection data are recorded in physical inspections that directly measure the component degradation. A Hidden Markov Gaussian Mixture Model (HM-GMM) is developed for modeling the condition monitoring data and a Bayesian network (BN) is developed to integrate the two data sources for DRA. Risk updating and prediction are exemplified on an Event Tree (ET) risk assessment model. A numerical case study and a real-world application on a Nuclear Power Plant (NPP) are performed to demonstrate the application of the proposed framework.

Keywords

Dynamic risk assessment (DRA), Condition monitoring data, Inspection data, Hidden Markov Gaussian Mixture model (HM-GMM), Bayesian network (BN), Probabilistic Risk Assessment (PRA), Prognostic and Health Management (PHM), Event Tree (ET), Nuclear Power Plant (NPP).

Acronyms

ATWS	Anticipated Transient Without Scram
BN	Bayesian Network
DRA	Dynamic Risk Assessment
EM	Expectation Maximization
ETA	Event Tree Analysis
FTA	Fault Tree Analysis
HM-GMM	Hidden Markov Gaussian Mixture Model
IE	Initialing Event
NPP	Nuclear Power Plant
PF	Particle Filtering

Notation

A	Transition probability matrix
$\boldsymbol{\pi}$	Initial state distribution of the Markov degradation process
$b_i(\mathbf{x})$	Probability distribution of the degradation indicator $\mathbf{x}$ when the degradation state is S_i
C_i	The i- th consequence in the ET
$\mathrm{c}_i(t_k)$	Condition monitoring data from the i- th safety barrier at $t = t_k$
$\mathbf{c}_{Tr}^{(k)}(t)$	Condition monitoring data from the k- th training sample at t
$d(\cdot)$	Euclidean distance
$f_{ET}(\cdot)$	ET model
K	Number of safety barriers with time-dependent failure probabilities
M	Number of safety barriers in a system
N	Number of consequences in the ET
$n_{feature}$	Number of features extracted from condition monitoring data
n_{Tr}	Number of samples in the training data set
P_{C_i}	Probability that consequence i occurs, given that the initialing event has occurred
$P_{CM,t_k}(S_{CM})$	Posterior distribution of the estimated degradation state from condition monitoring data, evaluated at

		t_k
$P_{INT,t_k}(S)$		Posterior distribution of the estimated degradation state by integrating condition monitoring data and inspection data, evaluated at t_k
Q		Number of health states
R_{IN}		Reliability of the inspection
R_{SB_M}		Reliability of the M-th safety barrier
S_{CM}		Estimated degradation state from condition monitoring data
$S_{CM,MAP}$		Most likely degradation state given the condition monitoring data
S_{IN}		Estimated degradation state from inspection data
S		True degradation state
t_{Tr}		Length of the observation period for the training samples
W		Working set that contains all the working states
$\mathbf{x}_{Tr}^{(k)}(t)$		Health indicator of k-th training data at t
$\mathbf{x}(t)$		Health indicator of safety barrier at t
$\boldsymbol{\mu}$		Vector of the mean values of the multivariate Gaussian distribution
$\boldsymbol{\Sigma}$		Covariance matrices of the multivariate Gaussian distribution
$\alpha_t(S_i)$		Forward variable
$\beta_t(S_i)$		Backward variable

1. Introduction

Probabilistic Risk Assessment (PRA) is widely applied to critical systems like space shuttles, nuclear power plants, etc [1]. Traditional PRA methods, like Event Tree Analysis (ETA) and Fault Tree Analysis (FTA), assume that the failure probabilities of the safety barriers are independent on time and their values are estimated based on statistical data [2]. However, in practice, the safety barriers undergo degradation processes like wear [3], fatigue [4], crack growth [5], etc., which increase their failure probabilities with time. Furthermore, the operational and environmental conditions of the system change with time and can also lead to time-dependent failure probabilities of the safety barriers [6, 7].

Safety barriers are the physical and/or non-physical means installed in the system of interest, aiming to prevent, control, or mitigate undesired events or accidents [8]. Examples are, a sprinkler system in a chemical plant [9], a reactor trip system in a nuclear power plant (NPP) [10]. To account for the time-dependent failure behavior of safety barriers, Dynamic Risk Assessment (DRA) frameworks have been developed, which use data and information collected during the system life to update the estimated risk indexes [11]. Bayesian theory has been used to update the probabilities of the events in an ET [12, 13]. Near miss and precursor data have been exploited in a hierarchical Bayesian model of DRA for the offshore industry [14, 15]. A real-time DRA has been performed in [16, 17], based on a dynamic loss function that considers multiple key state variables in the process industry. In [18], BN and Bow-tie model have been employed for the dynamic safety assessment of a natural gas station. A condition-based PRA has been performed in [6] for a spontaneous steam generator tube rupture accident. A data-driven DRA model has been developed for offshore drilling operations, where real time operational data have been used to update the probability of the kick event [19]. In [20], statistical failure data and condition monitoring data have been integrated in a hierarchical Bayesian model for DRA. DRA of an ET has been developed in [10] by using condition monitoring data to update the events probabilities.

In the existing methods, the data used for DRA can be broadly divided into two categories: statistical failure data and condition monitoring data. Statistical failure data refer to counts of accidents, incidents or near misses collected from similar systems [21]. For instance, in [22] and [23], DRA has been performed using near misses and incident data from similar processes. In [24], Bayesian theorem has been applied to update the failure probabilities of the safety barriers in a Bow-tie model for DRA. Statistical failure data are collected from a population of similar systems, which are seldom available in large number and this limits the application of the statistical failure data-based DRA methods in practice. Also, statistical data refer to a population of similar systems and do not

necessarily capture the plant-specific features of the target system. To address these issues, condition monitoring data are often used in DRA. Condition monitoring data refer to the online monitoring data collected by sensors that are installed in the target system for monitoring the degradation process of the safety barrier. For example, a condition-based fault tree has been used for DRA, where the condition monitoring data have been used to update the failure rates of the specific components and predict the reliability [25, 26]. Particle filtering (PF) has been used for DRA based on condition monitoring data from a nonlinear non-Gaussian process [27]. In [28], a Bayesian reliability updating method has been developed by using condition monitoring data considering the dependencies between two components. In [5], condition monitoring data from a passive safety system have been used for DRA, without considering the uncertainty in the condition monitoring data.

Inspection data are collected by physical inspections performed by maintenance personnel [29]. They have been widely used for online reliability assessment. For example, a Bayesian method has been developed to merge experts' judgment with continuous and discontinuous inspection data for the reliability assessment of multi-state systems [30]. A two-stage recursive Bayesian approach has been developed in [31], in order to update system reliability based on imperfect inspection data. Condition monitoring data and inspection data on wind turbine blades have been used separately for remaining useful life estimation in [32]. As inspections directly measure the component degradation, they provide valuable information complementary to condition monitoring data for DRA and can help reducing the impact of the uncertainty in the condition monitoring data on the result of DRA. However, to the best of our knowledge, no previous work has considered integrating condition monitoring data and inspection data for DRA.

In this paper, we develop a new framework to integrate condition monitoring data and inspection data in DRA. Compared to the existing works, the original contributions lie in:

(1) a Hidden Markov-Gaussian Mixture Model is developed for modeling condition monitoring data;

(2) a Bayesian network model is developed to integrate condition monitoring data and inspection data for DRA;

(3) a real-world application is performed.

The rest of the paper is organized as follows. Sect. 2 introduces the engineering motivation and formally defines the problem. In Sect. 3, a HM-GMM is developed for reliability updating and prediction of the failure of safety barriers based on condition monitoring data. A Bayesian network model is developed in Sect. 4 to integrate the inspection data and condition monitoring data for DRA. The framework is tested in Sect. 5 through a numerical

example. In Sect. 6, it is applied for the DRA of a real-world NPP. Finally, conclusions and potential future works are discussed in Sect. 7.

2. Problem definitions

The framework developed in this paper is motivated by real-world PRA practices. We consider an event tree model developed for the PRA of an Anticipated Transient Without Scram (ATWS) accident of a NPP [2]. The occurrence probabilities of the basic events, associated to the reliability of the safety barriers in the ET, are estimated from statistical data and assumed to remain constant throughout the life of the NPP [2]. However, the safety barriers in practice degrade. For example, a safety barrier in the aforementioned ET is the recirculation pump [2]; according to [33], most failures of the recirculation pump are caused by the degradation of the bearings, which makes the reliability of the pump time-dependent. DRA is best suited to capture such time-dependencies.

Two types of data can be used for the DRA of the ATWS accident. The first is inspection data. Take the bearing mentioned above as an example: through inspections, the degradation state of the bearing can be identified, e.g., healthy, minor degradation (e.g., outer race defect), medium degradation (e.g., roller element defect), severe degradation (e.g., inner race defect), etc. (see Figure 1). The second type of data is condition monitoring data: some observable signals, e.g., temperature, vibration, etc., that contain information on the degradation process are measured and used to infer the degradation state. For example, the vibration signals of bearings are often used as condition monitoring data to estimate the degradation state and update the reliability of bearings [34]. Inspection data usually give discrete degradation states, with uncertainty due to state classification by the maintenance operator. Condition monitoring data are subject to uncertainty due to observation noises and degradation state estimation errors. In this paper, a new framework is proposed to integrate condition monitoring data and inspection data for improving the accuracy and reducing the uncertainty of the risk assessment.

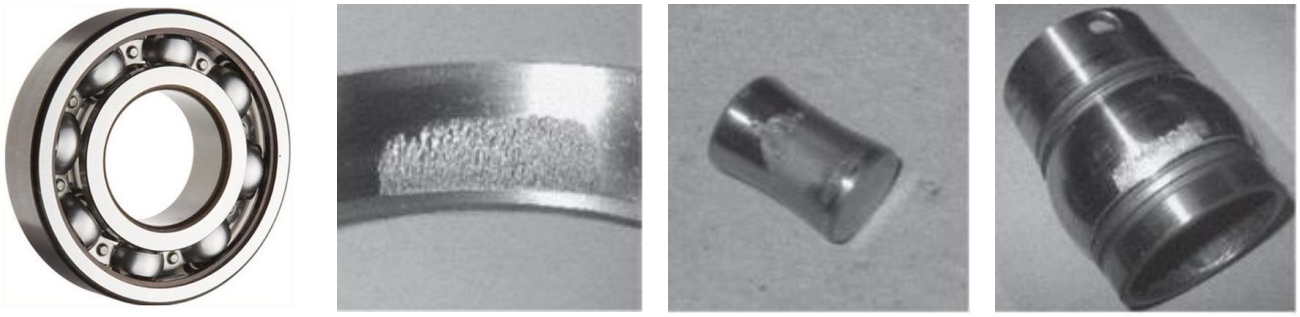

(a) healthy state (b) minor degradation (outer race defect) (c) medium degradation (roller element defect) (d) severe degradation (inner race defect)

Figure 1 Degradation states of bearing [35].

Without loss of generality, we consider a generic Even Tree (ET) model for DRA, but the framework is

applicable to other risk assessment models as well. Let IE represent the initialing event of the ET and assume that there are M safety barriers (SB) in the ET, denoted by $SB_i, i=1,2,\cdots,M$, whose states can be working or failure. The sequences that emerge from the IE depend on the states of the SBs and lead to N possible consequences, denoted by $C_1, C_2, \cdots, C_N$. The generic risk index considered in this paper is the conditional probability that a specific consequence C_i occurs, given that the IE has occurred:

$$P_{C_i} = P\{C_i \text{ occurs} \mid IE \text{ has occured}\}, i=1,2,\cdots,N. \tag{1}$$

Conditioning on the occurrence of the IE, these probabilities are functions of the reliabilities $R_{SB_i}, i=1,2,\cdots,M$ of the safety barriers along the specific sequences:

$$P_{C_i} = f_{ET}(R_{SB_1}, R_{SB_2}, \cdots, R_{SB_M}), i=1,2,\cdots,N. \tag{2}$$

where $f_{ET}(\cdot)$ is the ET model function. For example, in the ET in Figure 2, the risk index P_{C_2} of the consequence C_2 of the second accident sequence, in which the IE occurs with certainty, the first SB_1 functions successfully and the second SB_2 fails to provide its function, can be calculated as:

$$\begin{aligned} P_{C_2} &= f_{ET}(R_{SB_1}, R_{SB_2}) \\ &= R_{SB_1}(1-R_{SB_2}). \end{aligned} \tag{3}$$

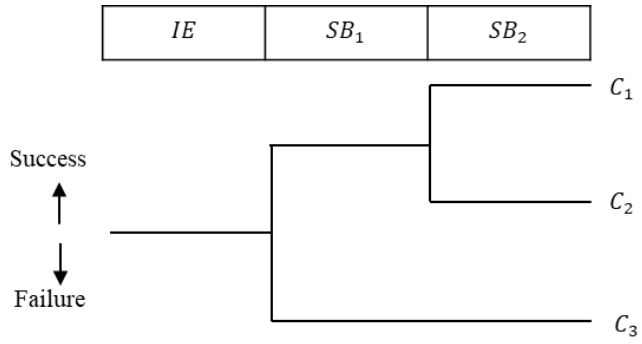

Figure 2 Illustrative Event Tree model.

Without loss of generality, we assume that in the ET:

(1) Safety barriers $SB_1, SB_2, \cdots, SB_K$ are subject to degradation processes and, therefore, their reliability functions are time-dependent, whereas $SB_{K+1}, SB_{K+2}, \cdots, SB_M$ do not degrade and have constant reliability values;

(2) Condition monitoring data are collected for $SB_1, SB_2, \cdots, SB_K$ at predefined time instants $t=t_k, k=1,2,\cdots q$;

(3) The collected condition monitoring data on the i-th safety barrier at $t = t_k$ are denoted by $c_i(t_k)$, where $i = 1,2,\cdots,K, k = 1,2,\cdots,q$ and $\mathbf{c}_i(t) = [c_i(t_1), c_i(t_2), \cdots, c_i(t_q)]$ is a vector containing all the signals that are monitored, where q is the length of the time series;

(4) At $t = t_{In}$, inspections are performed on the safety barriers $SB_i, i = 1,2,\cdots,K$. The inspection data are denoted by $S_{IN,i}, i = 1,2,\cdots,K$.

The DRA tasks are formally defined as:

(1) risk updating: at time $t = t_k, k = 1,2,\cdots,q$, update the estimated risk indexes at the current time t_k, based on the integration of condition monitoring and inspection data available up to t_k;

(2) risk prediction: at time $t = t_k$, predict the values of the risk indexes at future times, based on the integration of condition monitoring and inspection data available up to t_k.

3. A Hidden Markov Gaussian Mixture Model for modeling condition monitoring data

In this section, we develop a HM-GMM to model condition monitoring data. In Sect. 3.1, we formally define the HM-GMM. Then, in Sect 3.2, we show how to use the developed HM-GMM to estimate the degradation state of a safety barrier using condition monitoring data. The estimated degradation states are, then, used in Sect. 4 for data integration in DRA.

3.1 Model formulations

Without loss of generality, we illustrate the HM-GMM using the i-th safety barrier in the ET. For simplicity of presentation, we drop the subscript i in the notations. An illustration of the model is given in Figure 3. It is assumed that the safety barrier degrades during its lifetime and the degradation process follows a discrete state discrete time Markov model $S(t)$ with a finite state space $S(t) \in \{S_1, S_2, \cdots, S_Q\}$, where $S(t)$ represents the health state of the safety barrier, Q is the number of health states, and $S_1, S_2, \cdots, S_Q$ are in descending order of health (S_1 is the perfect functioning state, S_Q is the failure state). The evolution of the degradation process is characterized by the transition probability matrix of the Markov process, denoted by A, where $A = \{a_{ij}\}$ and $a_{ij} = P\left(S(t_{k+1}) = S_j \middle| S(t_k) = S_i\right), k = 1,2,\cdots,q, 1 \le i, j \le Q$. The initial state distribution of the Markov process is denoted by $\boldsymbol{\pi} = \begin{bmatrix} \pi_1 & \pi_2 & \cdots & \pi_Q \end{bmatrix}$, where $\pi_i = P\left(S(t_0) = S_i\right), 1 \le i \le Q$. It should be noted that repairs are not considered in this paper, just to simplify the calculation. Then, $S(t)$ can only transit to a worse state and cannot

move backwards to a better state. Besides, the failure state S_Q is an absorbing state, such that $p\left(S(t_{k+1})=i \middle| S(t_k)=S_Q\right)=1$ if and only if $i=S_Q$ and $p\left(S(t_{k+1})=i \middle| S(t_k)=S_Q\right)=0$ for all other values of i. However, the model accommodates the case of repairable components, where the transition matrix has non-zero entries also for backward state transitions, which represent the repairs of the safety barriers. The developed algorithms, can, then, be extended naturally.

The discrete time discrete state Markov process model is chosen because it is widely applied for quantitatively describing discrete state degradation processes in many practical applications [36]. For example, a discrete state Markov model has been used to model the bearing degradation process in [35]. The degradation process of a safety instrumented system is modeled by a Markov model for availability analysis [37, 38]. Although only Markov process-based degradation models are discussed in this paper, the developed methods for data integration into DRA can be easily extended to other degradation models.

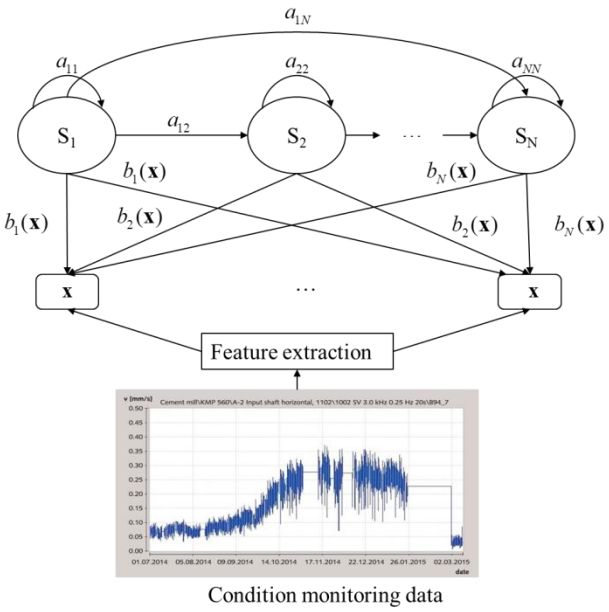

Figure 3 Description of the HM-GMM.

As described in Sect. 2.1, condition monitoring data $\mathbf{c}(t)$ are available at $t=t_k, k=1,2,\cdots,q$. In practice, $\mathbf{c}(t)$ contains only raw signals, which cannot be directly used for degradation modeling and analysis. Feature extraction, as shown in Figure 3, is needed to extract degradation features from $\mathbf{c}(t)$. For example, vibration signals are usually used as condition monitoring data for bearings [24]. The raw vibration signals, however, need to be preprocessed to extract features for degradation characterization. The commonly used degradation features include entropy, root mean square (RMS), kurtosis, etc [39]. In this paper, we refer to these extracted features as

degradation indicators and denote them by $\mathbf{x}(t)$, where $\mathbf{x}(t)=\left[x_1(t),x_2(t),\cdots,x_{n_{feature}}(t)\right]$ and $n_{feature}$ is the number of the degradation features.

As the safety barrier degrades, the degradation indicator $\mathbf{x}(t)$ exhibits distinct patterns. To capture such patterns and the uncertainty associated with them, it is assumed that at each degradation state $S_i, 1\le i\le Q,$ the values of the degradation indicators $\mathbf{x}$ follow a multivariate Gaussian distribution $b_i(\mathbf{x})=p(\mathbf{x}|S(t)=S_i)=N(\mathbf{x}|\boldsymbol{\mu}^{(i)},\boldsymbol{\Sigma}^{(i)}), i=1,2,\cdots,Q,$ as shown in Figure 3. The mean values vector $\boldsymbol{\mu}^{(i)}$ captures the degradation pattern at each degradation state, while the covariance matrix $\boldsymbol{\Sigma}^{(i)}$ captures the uncertainty in the condition monitoring data. An overall picture of the HM-GMM is given in Figure 3. Conceptually, we denote the HM-GMM compactly as $\boldsymbol{\lambda}=\{\boldsymbol{\pi},A,\boldsymbol{\mu},\boldsymbol{\Sigma}\}$, where $\boldsymbol{\pi}$ is the initial state distribution, A is the transition probability matrix, $\boldsymbol{\mu}=\left[\boldsymbol{\mu}_1,\boldsymbol{\mu}_2\cdots,\boldsymbol{\mu}_Q\right]$ is a vector of the mean values and $\boldsymbol{\Sigma}=\left[\Sigma^{(1)},\Sigma^{(2)},\cdots,\Sigma^{(Q)}\right]$ is a collection of the covariance matrices of the multivariate Gaussian distribution, respectively.

3.2 Degradation states estimation based on condition monitoring data

In this section, we show how to estimate the degradation states of the safety barriers based on the developed HM-GMM of the condition monitoring data. As shown in Figure 4, the estimation is made by an offline step and an online step. In the offline step, a HM-GMM is trained based on training data from a population of similar systems. The trained HM-GMM model, is, then, used in the online step for degradation state estimation based on the condition monitoring data.

The offline step starts from collecting training data, denoted by $\mathbf{c}_{Tr}^{(k)}(t), k=1,2,\cdots,n_{Tr}, t=t_1,t_2,\cdots,t_{Tr}$. The training data comprise of historical measurements of the degradation signals from a population of similar systems. To ensure the accuracy of HM-GMM training, it is required to collect as many as possible training samples, i.e., the sample size n_{Tr} should be as large as possible. The raw training data are preprocessed in a feature extraction step, as shown in Figure 4, to extract the health indicators $\mathbf{x}_{Tr}^{(k)}(t), k=1,2,\cdots,n_{Tr}, t=t_1,t_2,\cdots,t_{Tr}$. Depending on the nature of the degradation process condition, different feature extraction methods, e.g., time-domain, frequency domain, time-frequency analyses, etc., can be used [39]. Next, in the HM-GMM training step, the extracted degradation indicators are used to estimate the parameters $\boldsymbol{\lambda}=\{\pi,A,\boldsymbol{\mu},\boldsymbol{\Sigma}\}$ of the trained HM-GMM. In this paper, the Expectation Maximization (EM) algorithm [40] is employed for training the HM-GMM (see Sect. 3.2.1 for details).

The parameters $\boldsymbol{\lambda}$ is the output of the offline step.

The online step starts from collecting the condition monitoring data for the safety barrier, denoted by $\mathbf{c}(t_k), k=1,2,\cdots,q.$ The condition monitoring data should be of the same type and collected by the same sensors, as in the offline step. Then, the raw degradation signals are preprocessed and the health indicators $\mathbf{x}(t_k), k=1,2,\cdots,q$ of the target safety barrier are extracted, following the same procedures as in the offline step. Next, the degradation state of the safety barrier is estimated, based on the HM-GMM trained in the offline step. In this paper, we use the forward algorithm for degradation state estimation [40], as presented in details in Sect. 3.2.2. The estimated degradation state based on only condition monitoring data, denoted by $S_{CM}(t_k)$, is, then, integrated with inspection data for DRA in Sect. 4.

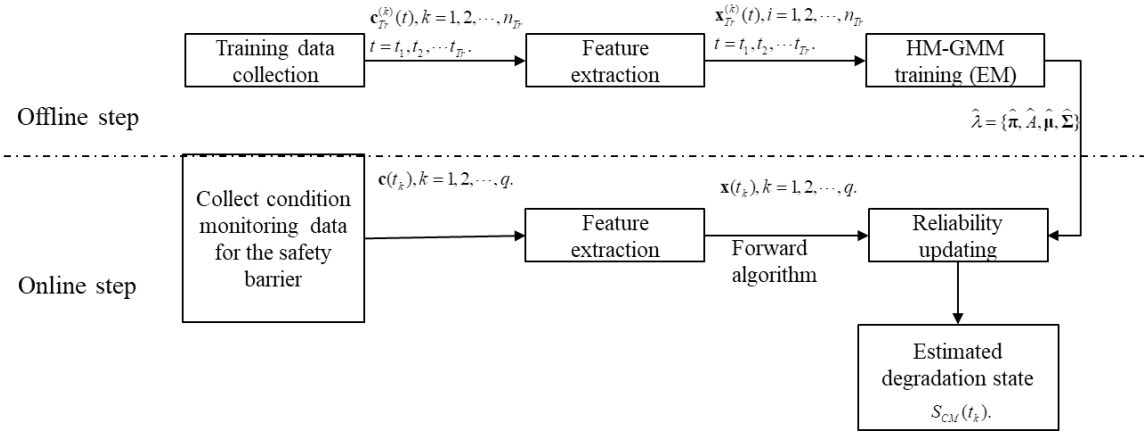

Figure 4 Degradation state estimation based on condition monitoring data.

3.2.1 HM-GMM training

In this section, we present in detail how to do HM-GMM training in the offline step. The parameters $\boldsymbol{\lambda}=\{\pi, A, \boldsymbol{\mu}, \boldsymbol{\Sigma}\}$ are estimated by maximizing the likelihood of observing the $\mathbf{x}_{Tr}^{(k)}(t), k=1,2,\cdots,n_{Tr}, t=t_1,t_2,\cdots,t_{Tr}$:

$$\begin{aligned}\boldsymbol{\lambda} &= \arg\max_{\boldsymbol{\lambda}} P\left(\mathbf{x}_{Tr}^{(1)}(t),\mathbf{x}_{Tr}^{(2)}(t),\cdots,\mathbf{x}_{Tr}^{(n_{Tr})}(t)\middle|\boldsymbol{\lambda}\right)\\ &= \arg\max_{\boldsymbol{\lambda}} \prod_{k=1}^{n_{Tr}} P\left(\mathbf{x}_{Tr}^{(k)}(t)\middle|\boldsymbol{\lambda}\right)\end{aligned} \tag{4}$$

Let $L \triangleq \prod_{k=1}^{n_{Tr}} P\left(\mathbf{x}_{Tr}^{(k)}(t)\middle|\boldsymbol{\lambda}\right)$ be the likelihood function of the observation data. Directly solving (4) is not possible in practice, as the likelihood function in (4) contains unobservable variables (the true degradation states $S(t)$ in this case). Expectation Maximization (EM) algorithm [40] is applied to solve this problem, where the maximum likelihood estimator is found in an iterative way: the current values of the parameters are used to estimate the unobservable variables (Expectation phase); then, the estimated values of the unknown variables are substituted

into the likelihood function to update the maximum likelihood estimators of the parameters (Maximization phase). The iterative procedures are repeated until the maximum likelihood estimators converge.

To apply the EM algorithm to the HM-GMM model, two auxiliary variables need to be defined first, i.e., forward variable $\alpha_t(S_i)$ and backward variable $\beta_t(S_i)$. The forward variable is defined as the probability of observing the health indicators up to the current time t and that the true degradation state $S(t)=S_i$, given a known HM-GMM $\boldsymbol{\lambda}$:

$$\alpha_t(S_i)=P(\mathbf{x}(t_1),\mathbf{x}(t_2),\cdots,\mathbf{x}(t),S(t)=S_i\,|\boldsymbol{\lambda}). \tag{5}$$

It is easy to verify that

$$\begin{aligned}&\alpha_1(S_i)=\pi_i b_i(\mathbf{x}(t_1)),\\ &\alpha_{t+1}(S_j)=b_j(\mathbf{x}_{t+1})\left[\sum_{i=1}^{Q}\alpha_t(S_i)a_{ij}\right],1\le i\le Q,1\le j\le Q,1\le t\le t_{Tr}\text{-}1,\end{aligned} \tag{6}$$

where t_{Tr} represents the observation time length and all the elements in π_i are zero, except the one that corresponds to the i-th element being one.

The backward probability $\beta_t(S_i)$ is defined as the probability of observing the health indicator $\mathbf{x}(t+1),\mathbf{x}(t+2),\cdots,\mathbf{x}(t_{Tr})$ from $t+1$ to the end of the observations, given that $S(t)=S_i$ and the model parameters are $\boldsymbol{\lambda}$:

$$\beta_t(S_i)=P(\mathbf{x}(t+1),\mathbf{x}(t+2),\cdots,\mathbf{x}(t_{Tr})\,|S(t)=S_i,\boldsymbol{\lambda}). \tag{7}$$

It is easy to verify that $\beta_t(S_j)=\left[\sum_{i=1}^{Q}b_j(\mathbf{x}(t+1))a_{ij}\right]\beta_{t+1}(S_j),1\le i,1\le j\le Q,\beta_{t_{Tr}}(i)=1,t=t_{Tr}-1,t_{Tr}-2,\cdots,1.$

The iterative estimators for the transition probabilities, denoted by a_{ij}, can, then, be derived as follows [41]:

$$a_{ij}=\frac{\sum_{k=1}^{n_{Tr}}\sum_{t=1}^{t_{Tr}}\xi_{Tr,t}^{(k)}(S_i,S_j)}{\sum_{k=1}^{n_{Tr}}\sum_{t=1}^{t_{Tr}}\gamma_{Tr,t}^{(k)}(S_i)}, \tag{8}$$

where $\xi_{Tr,t}^{(k)}(S_i,S_j)$ represents the probability of the k-th sample being in S_i at time t and state S_j at time $t+1$, and is calculated by [41]:

$$\begin{aligned}\zeta_{Tr,t}^{(k)}(S_i,S_j)&=P\left(S(t)=S_i,S(t+1)=S_j\,\middle|\,\mathbf{x}_{Tr}^{(k)}(t+1),\boldsymbol{\lambda}\right)\\&=\frac{\gamma_{Tr,t}^{(k)}(S_i)a_{ij}b_{Tr,j}^{(k)}(\mathbf{x}_{Tr}^{(k)}(t+1))\beta_{Tr,t+1}^{(k)}(S_j)}{\beta_{Tr,t}^{(k)}(S_i)},\end{aligned} \tag{9}$$

where $\gamma_{Tr,t}^{(k)}(S_i)$ represents the probability of being in S_i at time t given the health indicator $\mathbf{x}_{Tr}^{(k)}(t)$ and $\boldsymbol{\lambda}$ for the k-th training sample:

$$\gamma_{Tr,t}^{(k)}(S_i)=\frac{\alpha_{Tr,t}^{(k)}(S_i)\beta_{Tr,t}^{(k)}(S_i)}{p(\mathbf{x}_{Tr}^{(k)}(t)|\boldsymbol{\lambda})}=\frac{\alpha_{Tr,t}^{(k)}(S_i)\beta_{Tr,t}^{(k)}(S_i)}{\sum_{i=1}^{Q}\alpha_{Tr,t}^{(k)}(S_i)\beta_{Tr,t}^{(k)}(S_i)}. \tag{10}$$

The estimator for the initial state probability $\pi_i, i=1,2,\cdots,Q$ is calculated by [40]:

$$\pi_i=\frac{\sum_{k=1}^{n_{Tr}}\gamma_{Tr,t}^{(k)}(S_i)}{n_{Tr}}. \tag{11}$$

The estimators of the mean value vectors are derived as [41]:

$$\boldsymbol{\mu}_i=\frac{\sum_{k=1}^{n_{Tr}}\sum_{t=1}^{t_{Tr}}\gamma_{Tr,t}^{(k)}(S_i)\mathbf{x}_{Tr}^{(k)}(t)}{\sum_{k=1}^{n_{Tr}}\sum_{t=1}^{t_{Tr}}\gamma_{Tr,t}^{(k)}(S_i)}. \tag{12}$$

Similarly, the covariance matrices of the Gaussian output are calculated by [41]:

$$\boldsymbol{\Sigma}_i=\frac{\sum_{k=1}^{n_{Tr}}\sum_{t=1}^{t_{Tr}}\gamma_{Tr,t}^{(k)}(S_i)(\mathbf{x}_{Tr}^{(k)}(t)-\boldsymbol{\mu}_i)(\mathbf{x}_{Tr,t}^{(k)}-\boldsymbol{\mu}_i)'}{\sum_{k=1}^{n_{Tr}}\sum_{t=1}^{t_{Tr}}\gamma_{Tr,t}^{(k)}(S_i)}. \tag{13}$$

Algorithm 1 below summarizes the procedures for training the HM-GMM based on the EM algorithm. In Algorithm 1, $\|\cdot\|$ measures the distance between the current and the previous estimators. In this paper, we use the absolute value for its calculation, and tol is the tolerance of the error. In this paper, we set $tol=1\times10^{-4}$.

Algorithm 1: HM-GMM training based on EM algorithm.

Inputs: $\boldsymbol{\lambda}_0=\{\boldsymbol{\pi}_0, A_0, \boldsymbol{\mu}_0, \boldsymbol{\Sigma}_0\}, \mathbf{x}_{Tr}^{(1)}(t), \mathbf{x}_{Tr}^{(2)}(t), \cdots, \mathbf{x}_{Tr}^{(n_{Tr})}(t)$;

Outputs: $\boldsymbol{\lambda}=\{\pi, A, \boldsymbol{\mu}, \boldsymbol{\Sigma}\}$;

Step 1: $\boldsymbol{\lambda}=\boldsymbol{\lambda}_0$;

Step 2: Expectation phase: calculate the forward and backward variables, based on (5) and (7), respectively, using the current value of $\boldsymbol{\lambda}$;

Step 3: Maximization phase: update $\boldsymbol{\lambda}$ based on (8), (11)-(13), respectively;

Step 4: If $\|\boldsymbol{\lambda}-\boldsymbol{\lambda}_{prev}\|<tol$, End;

Else, $\boldsymbol{\lambda}_{prev}=\boldsymbol{\lambda}$, go to Step 2.

3.2.2 Degradation state estimation

In this paper, the forward algorithm [40] is employed to estimate the degradation state of the safety barriers in the online step. Let S_{CM} denote the estimated degradation state from condition monitoring data and $\mathrm{P}_{CM,t_k}(S_{CM}), k=1,2,\cdots,q$ represent the posterior distribution of S_{CM} given the condition monitoring data up to t_k:

$$\mathrm{P}_{CM,t_k}(S_{CM}=S_i)=P\left(S(t_k)=S_i\left|\mathbf{x}(t_1),\mathbf{x}(t_2)\cdots,\mathbf{x}(t_k),\boldsymbol{\lambda}\right.\right) \tag{14}$$

The posterior probabilities defined in (14) can be easily calculated from the forward probabilities defined in (15):

$$\begin{aligned}\mathrm{P}_{CM,t_k}(S_{CM}=S_i)&=\frac{P\left(S(t_k)=S_i,\mathbf{x}(t_1),\mathbf{x}(t_2)\cdots,\mathbf{x}(t_k)\left|\boldsymbol{\lambda}\right.\right)}{P\left(\mathbf{x}(t_1),\mathbf{x}(t_2),\mathbf{x}(t_2)\cdots,\mathbf{x}(t_k)\left|\boldsymbol{\lambda}\right.\right)}\\&=\frac{\alpha_{t_k}(S_i)}{\sum_{i=1}^{Q}\alpha_{t_k}(S_i)}.\end{aligned} \tag{15}$$

In practice, the $\alpha_{t_k}(S_i)$ in (15) is calculated recursively, based on (5).

At each $t=t_k$, the most likely degradation state, denoted by $S_{CM,MAP}(t_k)$, is, then, determined by finding the state with maximal posterior probability:

$$S_{CM,MAP}(t_k)=\arg\max_{1\le i\le Q}\left[\mathrm{P}_{CM,t_k}(S_{CM}=S_i)\right], 1\le k\le q. \tag{16}$$

Algorithm 2 below summarizes the major steps used for estimating the degradation state.

Algorithm 2 Forward algorithm for degradation state estimation at $t=t_k$.

Input: $\boldsymbol{\lambda}=\{\pi,A,\boldsymbol{\mu},\boldsymbol{\Sigma}\},\alpha_{t_{k-1}}(S_i),i=1,2,\cdots,Q,\mathbf{x}(t_k)$;

Output: $\mathrm{P}_{CM,t_k}(S_{CM}),S_{CM,MAP}(t_k)$;

Step 1: Calculate $\alpha_{t_k}(S_i),i=1,2,\cdots,Q,$ by (6);

Step 2: Calculate the posterior probability $\mathrm{P}_{CM,t_k}(S_{CM})$ by (15);

Step 3: Estimate the degradation state $S_{CM,MAP}(t_k)$ by (16).

4 Integrating condition monitoring data with inspection data for DRA

In this section, we first show how to integrate the condition monitoring data with inspection data for reliability

updating and prediction of the safety barriers (Sect. 4.1). Then, in Sect. 4.2, we develop a DRA method based on the updated and predicted reliabilities.

4.1 A Bayesian network model for data integration

As in the previous sections, we illustrate the developed data integration method using the i-th safety barrier at $t = t_k$. For simplicity and to avoid confusion, we drop the i and t_k in the notations. To update and predict the reliability, one needs to estimate the degradation state first. Let S_{IN} denote the degradation state estimated from inspection data and S denote the true degradation state. In practice, S_{IN} is subject to uncertainty due to potential imprecision in the inspection and recording by the maintenance personnel. To model such uncertainty, in this paper, we assume that the reliability of inspection is R_{IN}, and that the maintenance personnel correctly identify the true degradation state with a probability R_{IN}, whereas an inspection error can occur with probability $(1-R_{IN})$. When an inspection error occurs, it is further assumed that the probabilities for each of the possible degradation states being erroneously identified as the true degradation state are equal to each other:

$$P(S_{IN} = S_i \,|\, S) = \begin{cases} R_{IN}, & S = S_i \\ \dfrac{1-R_{IN}}{Q-1}, & S \neq S_i, \end{cases} \tag{17}$$

where Q is the number of degradation states. It is should be noted that other inspection models might also be assumed, depending on the actual problem setting.

In this paper, a BN is developed to describe the dependencies among S, S_{IN}, S_{CM}, as shown in Figure 5. The BN in Figure 5 is constructed based on the assumption that given the true degradation state S, the estimated degradation state from condition monitoring data and inspection data are conditional-independent.

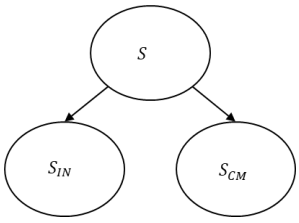

Figure 5 A BN model for data integration.

Based on the BN in Figure 5, we have

$$P(S, S_{IN}, S_{CM}) = P(S_{IN} \,|\, S) P(S_{CM} \,|\, S) P(S). \tag{18}$$

In (18), $P(S)$ measures the prior belief of the analysts on the current degradation states. We assume that $P(S)$

is a uniform distribution over all the possible degradation states, indicating that there is no further information to distinguish the states.

The conditional probability distribution $P(S_{IN}|S)$ describes the uncertainty in the inspections and is derived based on (17). In (17), the reliability of the inspection can be estimated from historical data or assigned based on expert judgments. The conditional probability distribution $P(S_{CM}|S)$ measures the trust one has on the estimated degradation state based on condition monitoring data. Its values can be estimated from validation test data. However, in practice, as validation tests are not always available, $P(S_{CM}|S)$ might also be assigned by experts considering the measurement uncertainty of the sensors and the distance between the neighboring degradation states. We give an example of how to determine $P(S_{CM}|S)$ in the case study of Sect. 6.

Once the condition monitoring data and inspection data are available, the observed values of S_{IN} and S_{CM} are known. Suppose we have $S_{CM}=S_j$ and $S_{IN}=S_i$. It should be noted that we choose the state with maximal posterior probability from (16) as the observation value of S_{CM}. The two data sources can be naturally integrated by calculating the posterior distribution of S given the two data sources, denoted by $P_{INT}(S)$. Based on the BN in Figure 5, we have:

$$\begin{aligned} P_{INT}(S) &\triangleq P\left(S \middle| S_{IN}=S_i, S_{CM}=S_j\right) \\ &= \frac{P\left(S, S_{IN}=S_i, S_{CM}=S_j\right)}{P\left(S_{IN}=S_i, S_{CM}=S_j\right)} \\ &= \frac{P\left(S_{IN}=S_i|S\right)P\left(S_{CM}=S_j|S\right)P(S)}{P\left(S_{IN}=S_i, S_{CM}=S_j\right)} \end{aligned} \tag{19}$$

Given the estimated posterior distribution in (19), the reliability of the safety barrier can be updated. Suppose the current time is t_k, the updated reliability can be calculated by:

$$R_{SB}(t_k)=\sum_{S\in W} \mathrm{P}_{INT,t_k}(S), \tag{20}$$

where W is the working set that contains all the working states; $\mathrm{P}_{INT,t_k}(S)$ is the posterior probability of the true degradation state after integrating the two data sources at $t=t_k$ and is calculated from (19).

Furthermore, at $t=t_k$, we can also predict the reliability of the safety barriers at a future time t_{Fut}. For this, the distribution of the degradation states at $t=t_{Fut}$ is predicted first, using Chapman-Kolmogorov equation [42] and the trained model from the offline step:

$$P_{INT,t_{Fut}}(S) = P_{INT,t_k}(S) \times A^{(t_{Fut}-t_k)}. \quad (21)$$

The reliability at $t = t_k$, can be predicted as:

$$R_{SB}(t_{Fut}) = \sum_{S \in W} P_{INT,t_{Fut}}(S). \quad (22)$$

4.2 Dynamic risk assessment

The updated reliabilities from (20), can, then, be substituted into (2) for DRA:

$$r_{C_i}(t_k) = f_{ET}(R_{SB_1}(t_k), R_{SB_2}(t_k), \cdots, R_{SB_K}(t_k), R_{SB_{K+1}}, \cdots, R_{SB_M} | IE), i = 1, 2, \cdots, N, \quad (23)$$

where in (23), $R_{SB_i}(t_k)$ is calculated by (20). Similarly, the risk index at a future time t_{Fut} can be predicted by:

$$r_{C_i}(t_{Fut}) = f_{ET}(R_{SB_1}(t_{Fut}), R_{SB_2}(t_{Fut}), \cdots, R_{SB_K}(t_{Fut}), R_{SB_{K+1}}, \cdots, R_{SB_M} | IE), i = 1, 2, \cdots, N, \quad (24)$$

where $R_{SB_i}(t_{Fut})$ is calculated by (21) and (22).

Figure 6 summarizes the major steps for the developed DRA method by integrating condition monitoring data with inspection data. It should be noted that in Figure 6, the risk updating is made at $t = t_k$, while risk prediction is made for a given future time t_{Fut}.

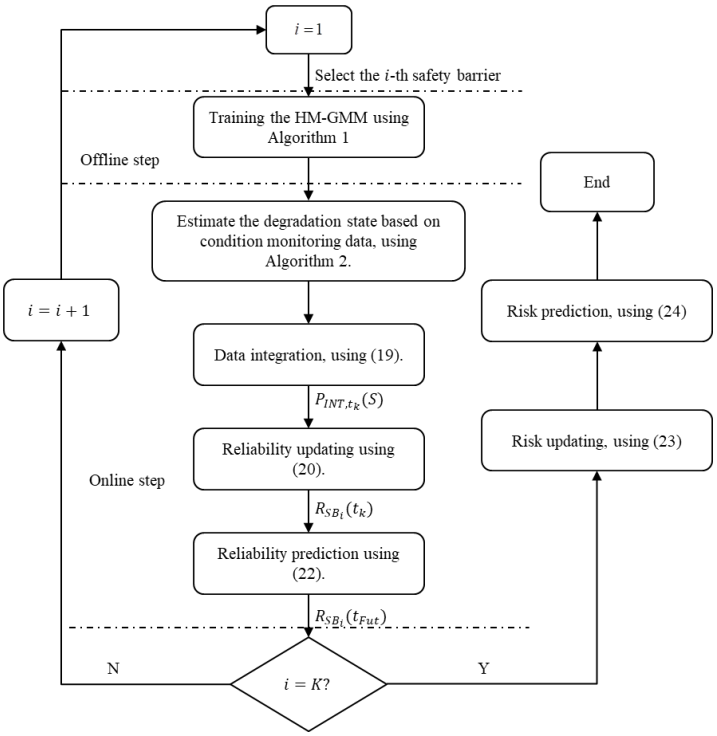

Figure 6 Procedures for DRA based on condition monitoring and inspection data.

5. Numerical case study

In this section, we apply the DRA framework for data integration (see Sect. 4.1) on a numerical case study.

The purpose is to test the updating and prediction of safety barrier reliability. Hence, only reliability updating and prediction are considered. The application of the overall DRA framework is done in Sect. 6 on a real-world case.

Consider a component whose degradation process follows a discrete state discrete time Markov chain $S(t)$ with four discrete degradation states S_1, S_2, S_3, S_4, where $S_1 \sim S_4$ have increasing degrees of degradation from S_1 perfect state, to S_4 failure state. The condition monitoring data are generated from a HM-GMM with known parameters values:

$$
\begin{aligned}
&\mathrm{A}=\begin{pmatrix} 0.6 & 0.2 & 0.1 & 0.1 \\ 0 & 0.5 & 0.25 & 0.25 \\ 0 & 0 & 0.5 & 0.5 \\ 0 & 0 & 0 & 1 \end{pmatrix}, \\
&\boldsymbol{\pi}=\begin{bmatrix} 1 & 0 & 0 & 0 \end{bmatrix}, \\
&\boldsymbol{\mu}=\begin{pmatrix} 0.0588 & 0.1424 & 0.1842 & 1 \\ 0.1268 & 0.1597 & 0.2432 & 1 \\ 0.0946 & 0.9744 & 0.8648 & 0.8449 \end{pmatrix}, \\
&\boldsymbol{\Sigma}^{(i)}=\begin{pmatrix} 0.001 & 0 & 0 \\ 0 & 0.001 & 0 \\ 0 & 0 & 0.001 \end{pmatrix}, \text{with } i=1,2,3,4.
\end{aligned}
\tag{25}
$$

The degradation indicator comprises of three features, denoted by x_1, x_2 and x_3, respectively. The size of the generated training data is 10^4 and $t = t_1, t_2, \cdots, t_{23}$ are the time instants of data collection. Then, the training data can be represented as $\mathbf{x}_{Tr}^{(k)}(t), k = 1, 2, \cdots, 10^4, t = t_1, t_2, \cdots, t_{23}$, where $\mathbf{x}_{Tr}^{(k)}(t) = \left[x_{Tr,1}^{(k)}(t), x_{Tr,2}^{(k)}(t), x_{Tr,3}^{(k)}(t) \right]$. The training data are used in the offline step for estimating the model parameters. Then, another sample, denoted by $\mathbf{x}_{CM}(t), t = 1, 2, \cdots, t_{CM}$, is generated from the HM-GMM in (25) and used as condition monitoring data collected on the safety barrier monitored in the online step, as shown in Figure 7.

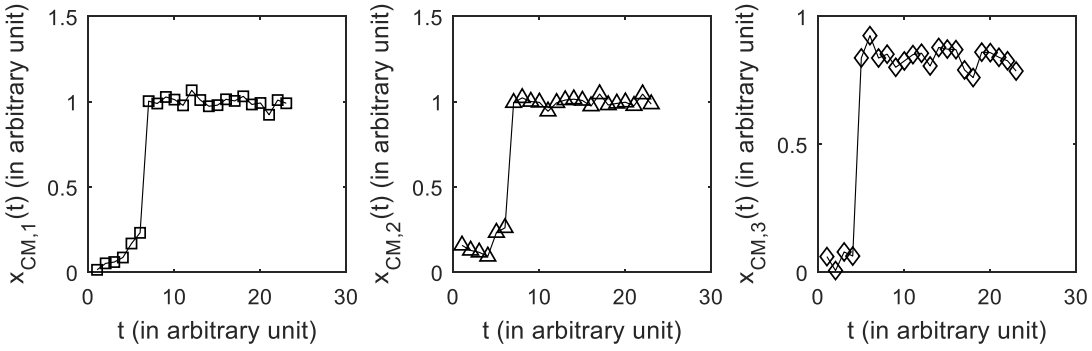

Figure 7 The generated condition monitoring data for the monitored safety barrier.

Based on the generated condition monitoring data, the reliability updating and prediction can be done using

Algorithm 1 and equations (20) and (22). Due to the noise in the condition monitoring data, the updated reliability is subject to uncertainty. The method in Figure 6 is applied to solve this problem by integrating condition monitoring data with inspection data. In this section, we test the performance of the developed data integration method under three possible scenarios:

(1) Both condition monitoring data and inspection data correctly estimate the degradation state: this scenario is represented by choosing the time point $t=t_3$, where the estimated degradation state from condition monitoring data and the true degradation state are both S_2. The inspection data at t_k is generated to be exactly $S_{IN}(t_3)=S_2$.

(2) Condition monitoring data correctly estimate the degradation state, but inspection data do not: this scenario is represented by choosing the time point $t=t_7$, where the estimated degradation state from condition monitoring data and the true state are both S_3, whereas the inspection data at t_7 is randomly sampled from $S_k, k=1,\cdots,Q, k\neq 3$. The state from the inspection data is $S_{IN}(t_3)=S_2$.

(3) Inspection data correctly estimate the degradation state, but condition monitoring data do not: this scenario is generated by choosing the time point $t=t_5$, where the estimated degradation state from condition monitoring data is $S_{CM}(t_5)=S_2$, whereas the true degradation state is $S(t_5)=S_3$. The inspection data at t_5 are generated to be $S_{IN}(t_5)=S(t_5)=S_3$.

In subsections 5.1-5.3, we apply the developed data integration method on the three scenarios above.

5.1 Scenario I: Both data sources are reliable

The reliability updating and prediction processes are conducted following the procedures in Figure 6, at $t=t_3$. The updated and predicted reliability are compared to those calculated based on only condition monitoring data and only inspection data, respectively. The comparison is shown in Figure 8. We also show the relative errors of the three methods with respect to the true values in Table 1.

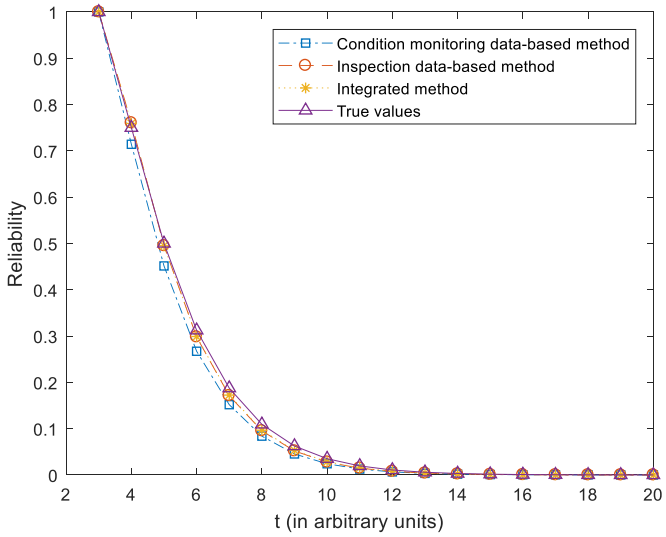

Figure 8 Updated and predicted reliability at $t = t_3$ (scenario I).

Table 1 Relative errors of the scenario I

	$t = t_3$	$t = t_4$	$t = t_5$	$t = t_6$	$t = t_7$	$t = t_8$	$t = t_9$	$t = t_{10}$
Condition monitoring data-based method	0	4.8%	9.7%	14.5%	19%	23%	27%	31%
Inspection data-based method	0	1.34%	0.9%	4.6%	8.7%	12.9%	17%	21%
Integrated method	0	1.2%	0.9%	4.3%	7%	11.7%	15%	18.6%

As shown in Figure 8 and Table 1, the proposed method provides a more accurate estimation and prediction of the reliability than the other two methods. This is because condition monitoring data are affected by noise from the data collection process, which results in uncertainty in the estimated degradation state. In this case, the state distribution estimated by the condition monitoring data is

$$P_{CM,t_3}(S_{CM}) = [0 \quad 0.8263 \quad 0.1737 \quad 0], \tag{26}$$

whereas the one estimated by integrating the two data sources is

$$P_{INT,t_3}(S) = [0.01 \quad 0.98 \quad 0.01 \quad 0]. \tag{27}$$

It can be seen that integrating the two data sources reduces the uncertainty in the degradation state estimation (note that at $t = t_3$, the true degradation state is S_2). Therefore, the updated and predicted reliabilities are more accurate than only using condition monitoring data.

On the other hand, the transition probability matrix A estimated from the offline step is

$$A = \begin{bmatrix} 0.6010 & 0.2125 & 0.0865 & 0.1 \\ 0 & 0.4483 & 0.3121 & 0.2395 \\ 0 & 0 & 0.4938 & 0.5062 \\ 0 & 0 & 0 & 1 \end{bmatrix}. \tag{28}$$

Comparing (28) to the true values in (25), it can be seen that when the current state is S_2, the estimated A tends to underestimate the reliability as it overestimates the transition probabilities to the failure states. As the inspection data estimate that the system is in S_2, using only inspection data tends to underestimate the reliability. Integrating the two data sources, as shown in (27), predicts that the safety barrier is also likely to be in S_1, which compensates the errors in the estimated λ and results in more accurate reliability estimates.

5.2 Scenario II: Condition monitoring data are reliable but inspection data are not

The reliability updating and prediction processes are conducted following the procedures in Figure 6, at $t = t_7$. The updated and predicted reliability are compared to those calculated based on only condition monitoring data and only inspection data, respectively. The comparison is shown in Figure 9. We also present the relative error of the three methods by comparing them to the true values in Table 2.

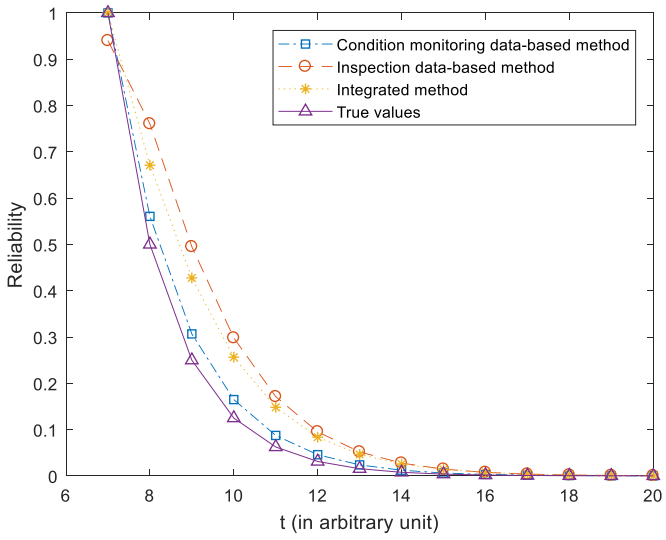

Figure 9 Updated and predicted reliability at $t = t_7$ (scenario II).

Table 2 Relative errors of the scenario II.

	$t = t_7$	$t = t_8$	$t = t_9$	$t = t_{10}$	$t = t_{11}$	$t = t_{12}$	$t = t_{13}$	$t = t_{14}$
Condition monitoring data-based method	0	12%	22%	33%	39%	46%	52%	57%
Inspection data-based method	0	52%	98%	138%	173%	204%	232%	255%
Integrated method	6%	34%	71%	96%	105%	137%	158%	197%

As shown in Figure 9 and Table 2, the results obtained by the inspection-data based method have the largest estimation error. The proposed data integration method provides more accuracy than the inspection data-based method. This is expected, as in this case the inspection data fail to correctly estimate the degradation state. By integrating condition monitoring data, the incorrect information from inspection data can be somewhat corrected.

On the contrary, the estimation error of the data integration method is larger than that of the condition monitoring data-based method. This is because the data integration method is affected by the incorrect information from the inspection data. Trustworthiness of the inspection becomes essential, then.

5.3 Scenario III: Inspection data are reliable but condition monitoring data are not

The reliability updating and prediction are conducted following the procedures in Figure 6, at $t = t_5$. The updated and predicted reliability are compared to those calculated based on only condition monitoring data and only inspection data, respectively. The comparison is shown in Figure 10. We also present the relative errors of the three methods by comparing them to the true values in Table 3.

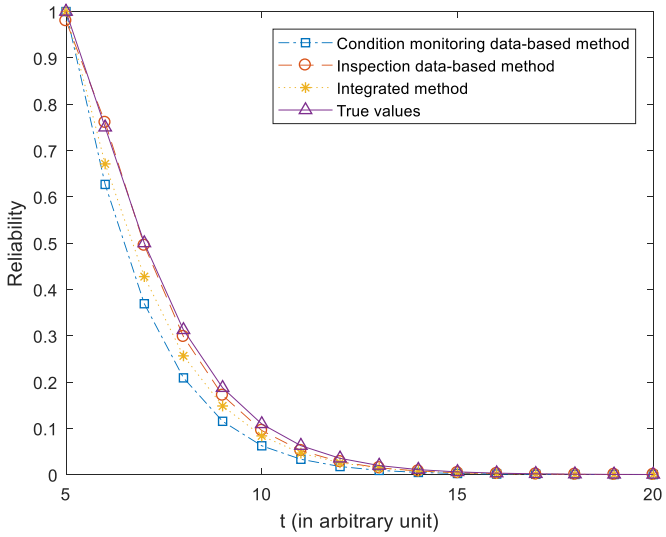

Figure 10 Updated and predicted reliability at $t = t_5$ (scenario III).

Table 3 Relative errors of the scenario III.

	$t = t_5$	$t = t_6$	$t = t_7$	$t = t_8$	$t = t_9$	$t = t_{10}$	$t = t_{11}$	$t = t_{12}$
Condition monitoring data-based method	0	16%	26%	14.5%	33%	38.5%	43%	46%
Inspection data-based method	0	1.39%	2.9%	4.6%	8.6%	12.9%	16.9%	21%
Integrated method	2%	10%	14%	17%	20%	23%	25%	27%

As shown in Figure 10 and Table 3, the results obtained by the condition monitoring data-based method have the largest estimation errors. This is expected as in this case, the condition monitoring data fail to correctly estimate the degradation state. The proposed data integration method provides a more accurate result than the condition monitoring data-based method. This is because, by integrating inspection data, the incorrect estimation from the condition monitoring data can be compensated. However, the estimation error is larger than that of the inspection data-based method. This is because the data integration method also considers the incorrect information from the condition monitoring data.

In practical operation, the developed method can help the stakeholder/decision-makers to determine when to perform preventive maintenance on critical safety barriers. This is done by setting a minimum acceptable value for reliability and calculating the first time the reliability drops below this value. However, the reliability estimation can sometimes be imprecise. The developed method, can, then, provide a more realistic assessment to support decision making regarding when a preventive replacement is needed.

6. Application

In this section, the developed method is applied for DRA of an Anticipated Transient Without Scram (ATWS) accident of a NPP [2]. The description of the case study is briefly introduced in Sect. 6.1. Then, in Sect. 6.2, the developed HM-GMM and the data integration process are presented. The results of the DRA are presented and discussed in Sect. 6.3.

6.1 System description

ATWS is an accident that can happen in a NPP. In this accident, the scram system, which is designed to shut down the reactor during an abnormal event (anticipated transient), fails to work [43]. An ET has been developed for PRA of the ATWS for a NPP in China [2], as shown in Figure 11. In Figure 11, T_1ACM represents the failure of the automatic scram system and is the initialing event (IE) considered. Eleven safety barriers ($SB_1 \sim SB_{11}$) are designed to contain the accident (Table 4). Depending on the states of the safety barriers, 23 sequences can be generated ($SE_{01} - SE_{23}$) [2, 44]. The consequences of the sequences are grouped into two categories, based on their severity; the first group,

$$C_s = \{SE_{03}, SE_{06}, SE_{07}, SE_{08}, SE_{09}, SE_{12}, SE_{13}, SE_{14}, SE_{15}, SE_{18}, SE_{19}, SE_{20}, SE_{21}, SE_{22}, SE_{23}\}, \quad (29)$$

represents the event sequences with severe consequences, whereas the remaining event sequences have non-severe consequences [44]. The risk index $Risk$ considered in this paper is the conditional probability of having severe consequences, given the initialing event ($IE = T_1 ACM$):

$$Risk \triangleq P(C_S \,|\, IE) = f_{ET}(R_{SB_1}, R_{SB_2}, \cdots, R_{SB_M} \,|\, T_1\, ACM), \quad (30)$$

where the model function $f_{ET}(\bullet)$ is determined from the ET in Figure 11 and $R_{SB_1}, R_{SB_2}, \cdots, R_{SB_M}$ are the reliabilities of the safety barriers, calculated based on the component failure probabilities in Table 4. It should be noted that the failure probabilities for SB_7 and SB_8 change depending on the event sequence that occurs (see,

e.g., $P^{(1)}_{f,SB_7}$ and $P^{(2)}_{f,SB_7}$ in Figure 11 and Table 4).

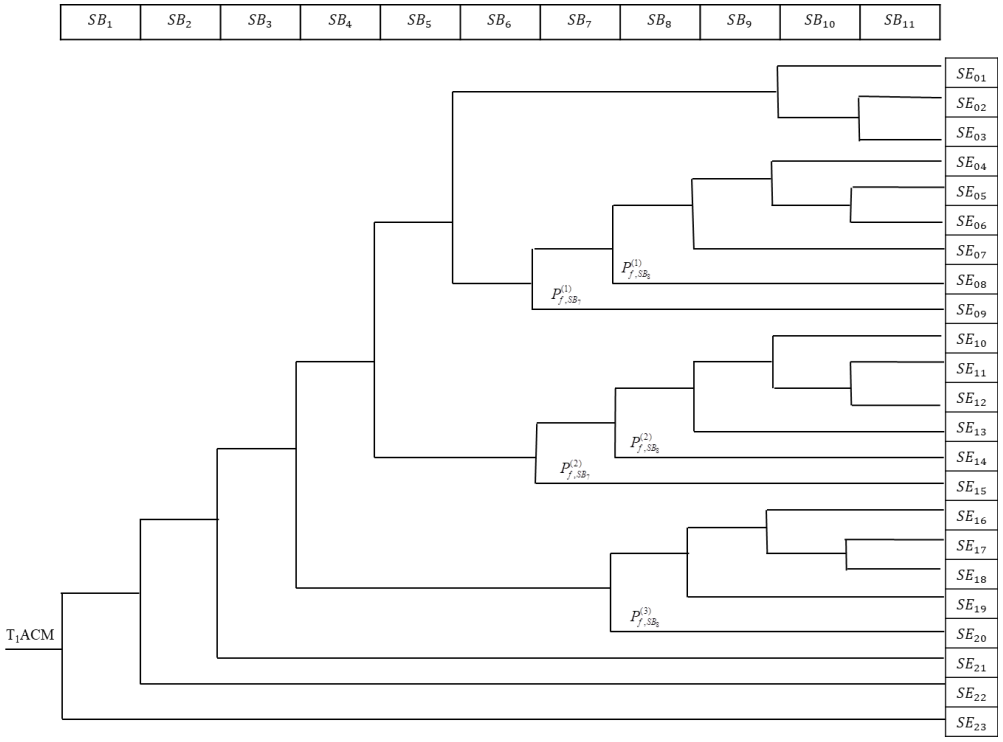

Figure 11 ET for the ATWS [44]; at each branching, the upper branch corresponds to the non-failure of the safety barrier and the low branch corresponds to the failure of the safety barrier.

In this original ETA of the ATWS, the failure probabilities in Table 4 are assumed to be constant values. In practice, however, these probabilities might change due to various degradation mechanisms. Take the recirculation pump as an example. According to [33], most field failures of the recirculation pump are caused by the degradation of the bearing inside the pump, which makes the failure probability of the recirculation pump time-dependent. In this paper, we make a DRA on the ET in Figure 11, considering the degradation of the bearing in the recirculation pump.

The condition monitoring data of the bearing come from the bearing degradation dataset from university of Cincinnati [45]. The dataset contains four samples and for each sample, raw condition monitoring data are collected in real time by measuring the vibration acceleration signals. An illustration of the raw data is given in Figure 12. On the other hand, the inspection can be performed at some given time instants to identify the different degradation states. As shown in Figure 1, we distinguish from four degradation states in this case study.

Table 4 Safety barriers in the target system [2].

Safety barrier	Failure probability (P_f)	Description
Recirculation pump (SB_1)	1.96×10^{-3}	Once the plant fails to scram, the recirculation pump is activated and used to limit power generation of the NPP.
Safety valve (SB_2)	1.01×10^{-5}	Safety valves are opened to prevent over-pressurization of the reactor.
Boron injection (SB_3)	1×10^{-5}	Liquid boron should be injected manually by the operator within the allowable time to shut down the reactor safely.
Automatic Depressurization System (ADS) inhibit (SB_4)	1.37×10^{-2}	ADS is designed to decrease the pressure of the reactor in order to start the low-pressure system.
Early high-pressure makeup (SB_5)	8.45×10^{-2}	The system is supposed to work automatically when automatic actuation alarm appears, indicating that the water level is lowering to level 2.
Long-term high-pressure makeup (SB_6)	2.13×10^{-3}	The long-term high-pressure system is used to maintain the water level in the vessel 24 hours after the start.
Manual reactor depressurization (SB_7)	$P_{f,SB_7}^{(1)}=0.45$, $P_{f,SB_7}^{(2)}=0.9$	The operator depressurizes the vessel manually to avoid core melt-down. In $SE_{04}-SE_{09}$, the failure probability is $P_{f,SB_7}^{(1)}$, whereas, in $SE_{10}-SE_{15}$, the failure probability is $P_{f,SB_7}^{(2)}$.
Reactor inventory makeup at low pressure (SB_8)	$P_{f,SB_8}^{(1)}=1.12\times10^{-6}$, $P_{f,SB_8}^{(2)}=3.4\times10^{-6}$, $P_{f,SB_8}^{(3)}=9.49\times10^{-5}$	If the low pressure system fails as well as the high-pressure system, then the reactor inventory makeup at lower pressure needs to be activated. In $SE_{04}-SE_{07}$, the failure probability is $P_{f,SB_8}^{(1)}$, while, in $SE_{10}-SE_{14}$, the failure probability is $P_{f,SB_8}^{(2)}$. In $SE_{16}-SE_{20}$, the failure probability is $P_{f,SB_8}^{(3)}$.
Vessel overfill prevention (SB_9)	0.875	The operator needs to monitor the water level and make sure the level is not too high to cause core melt-down.
Long-term heat removal (SB_{10})	2.03×10^{-5}	The long-term heat removal system is initialized to cool down the suppression pool and containment in order to maintain the other supporting systems in working states.
Vessel inventory makeup after containment (SB_{11})	0.4	This measure supplies the proper amount of water to protect the fuel from melting when containment failure happens.

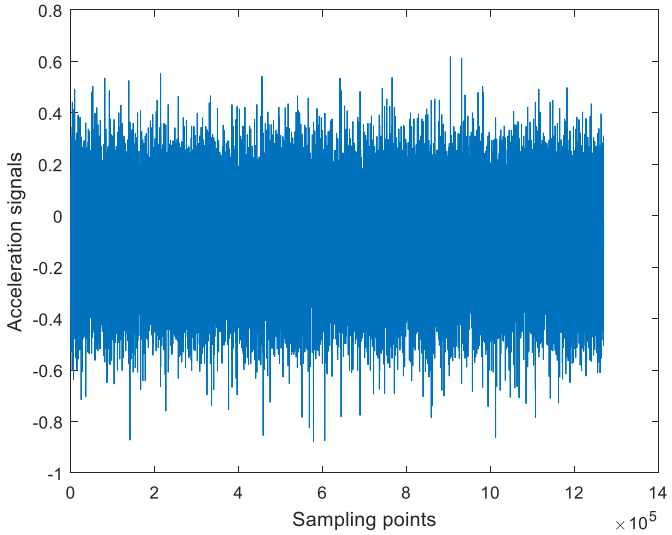

Figure 12 Raw data for the bearing 1 in the test #1 at 10 minutes.

6.2 Dynamic risk assessment

DRA of the ATWS is carried out following the procedures in Figure 6, where the real data set from [45] is used as historical training data. In the offline step, feature extraction needs to be conducted first. Three features are extracted from the vibration signals using the time domain method:

$$\begin{cases} x_1(t_i) = \dfrac{1}{(t_i - t_{i-1}) \cdot f} \sum\limits_{j \in (t_{i-1}, t_i)} {c_j}^2 \\ x_2(t_i) = \sqrt{\dfrac{1}{(t_i - t_{i-1}) \cdot f} \sum\limits_{j \in (t_{i-1}, t_i)} (c_j - \bar{c})^2} \\ x_3(t_i) = \dfrac{1}{(t_i - t_{i-1}) \cdot f} \sum\limits_{j \in (t_{i-1}, t_i)} c_j \end{cases} \tag{31}$$

where x_1 is the average power of vibration, x_2 is the root mean square, x_3 is the mean value of vibration. In (31), f is the sampling frequency, $(t_i - t_{i-1}) \cdot f$ is the number of sampling points in time interval $[t_{i-1}, t_i]$, and c_j is the vibration signal. The extracted degradation indicators are shown in Figure 13.

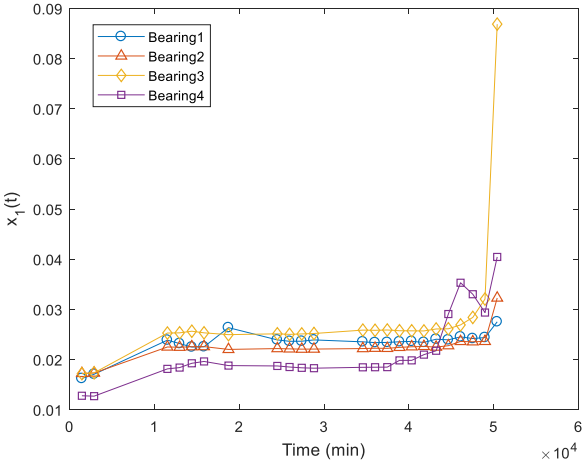

(a) $x_1(t)$: average power of vibration

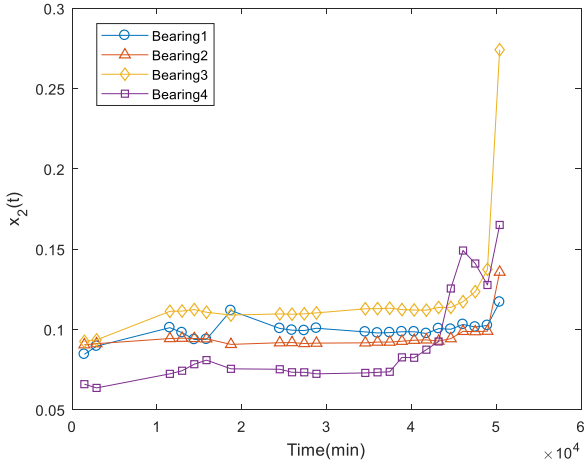

(b) $x_2(t)$: root mean square

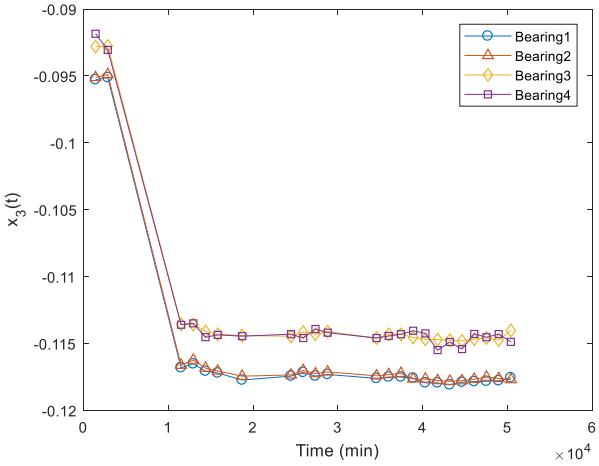

(c) $x_3(t)$: mean value of vibration

Figure 13 Extracted degradation indicators.

Algorithm 1 is applied to train a HM-GMM with four discrete degradation states based on the extracted degradation indicators:

$$A=\begin{pmatrix} 0.5 & 0.5 & 0 & 0 \\ 0 & 0.9354 & 0.0646 & 0 \\ 0 & 0 & 0.9565 & 0.0435 \\ 0 & 0 & 0 & 1 \end{pmatrix}, \pi = \begin{bmatrix} 1 & 0 & 0 & 0 \end{bmatrix},$$

$$\boldsymbol{\mu} = \begin{pmatrix} 0.0412 & 0.1176 & 0.2002 & 1.0000 \\ 0.0916 & 0.1184 & 0.2634 & 1.0000 \\ 0.0579 & 0.9168 & 0.8672 & 0.8446 \end{pmatrix}, \tag{32}$$

$$\boldsymbol{\Sigma}^{(1)} = \begin{pmatrix} 0.0108 & 0.0018 & 0.0007 \\ 0.0018 & 0.0137 & 0.0014 \\ 0.0007 & 0.0014 & 0.0121 \end{pmatrix}, \boldsymbol{\Sigma}^{(2)} = \begin{pmatrix} 0.0111 & 0.0020 & 0.0012 \\ 0.0020 & 0.0134 & 0.0019 \\ 0.0012 & 0.0019 & 0.0137 \end{pmatrix},$$

$$\boldsymbol{\Sigma}^{(3)} = \begin{pmatrix} 0.0129 & 0.0039 & 0.0002 \\ 0.0039 & 0.0153 & 0.0002 \\ 0.0002 & 0.0002 & 0.0106 \end{pmatrix}, \boldsymbol{\Sigma}^{(4)} = \begin{pmatrix} 0.01 & 0 & 0 \\ 0 & 0.01 & 0 \\ 0 & 0 & 0.01 \end{pmatrix}.$$

The online condition monitoring data are generated using the bootstrap sampling: 10^4 bootstrap samples are

generated from the training data set. A HM-GMM $\hat{\lambda}$ is, then, trained based on these samples using Algorithm 1:

$$
\begin{aligned}
&\mathrm{A}=\begin{pmatrix} 0.5 & 0.5 & 0 & 0 \\ 0 & 0.9613 & 0.0387 & 0 \\ 0 & 0 & 0.7150 & 0.2849 \\ 0 & 0 & 0 & 1 \end{pmatrix}, \pi = \begin{bmatrix} 1 & 0 & 0 & 0 \end{bmatrix}, \\
&\boldsymbol{\mu} = \begin{pmatrix} 0.0446 & 0.1338 & 0.2339 & 0.7809 \\ 0.0974 & 0.2004 & 0.3087 & 0.8062 \\ 0.0764 & 0.9744 & 0.8779 & 0.8584 \end{pmatrix}, \\
&\boldsymbol{\Sigma}^{(1)} = \begin{pmatrix} 0.0105 & 0.0010 & 0.0005 \\ 0.0010 & 0.0122 & 0.0009 \\ 0.0005 & 0.0009 & 0.0118 \end{pmatrix}, \boldsymbol{\Sigma}^{(2)} = \begin{pmatrix} 0.0109 & 0.0016 & 0.0007 \\ 0.0016 & 0.0128 & 0.0010 \\ 0.0007 & 0.0010 & 0.0128 \end{pmatrix}, \\
&\boldsymbol{\Sigma}^{(3)} = \begin{pmatrix} 0.0123 & 0.0030 & 0.0000 \\ 0.0030 & 0.0141 & -0.0001 \\ 0.0002 & -0.0001 & 0.0105 \end{pmatrix}, \boldsymbol{\Sigma}^{(4)} = \begin{pmatrix} 0.0111 & 0.0013 & 0.0001 \\ 0.0013 & 0.0116 & 0.0001 \\ 0.0001 & 0.0001 & 0.0100 \end{pmatrix}.
\end{aligned}
\tag{33}
$$

The HM-GMM λ in (33) is, then, treated as the true degradation model and used to generate the condition monitoring data for the bearing that is monitored in the online step. The generated condition monitoring data are shown in Figure 14.

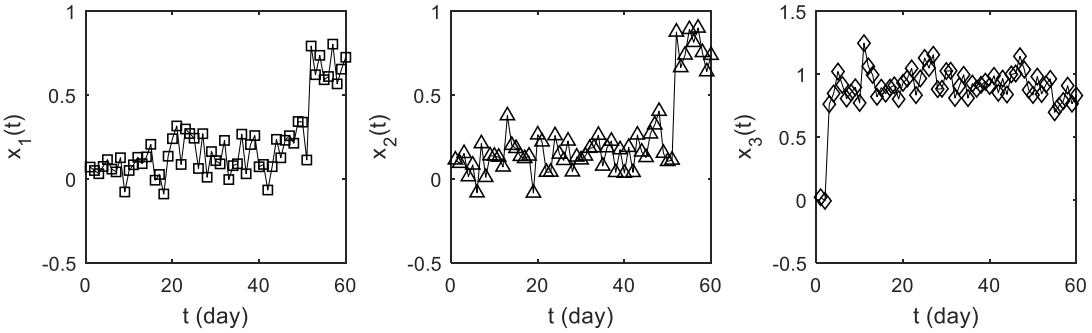

Figure 14 The generated condition monitoring data.

Inspections are conducted at three time instants, i.e., $t = 30(d)$, $t = 35(d)$ and $t = 50(d)$, respectively. The inspection data at the three time instants are given in Table 5. In Table 5, we also show the true degradation states obtained from the true degradation model in (33) and the estimated degradation states using condition monitoring data and Algorithm 2.

The estimated degradation state S_{IN} and S_{CM} are, then, integrated using (19). Note that in (17), the reliability of the inspection data is set to $R_{IN} = 0.8$. Then, the value of $P(S_{IN}|S)$ in (19) can be derived easily from (17). The values of $P(S_{CM}|S)$ are assigned by considering the distance between the neighboring degradation states: the closer the states are, the more likely a misclassification might happen. For example, the normalized distance between S_2 and S_3 is:

$$\frac{d\left(\boldsymbol{\mu}_2,\boldsymbol{\mu}_3\right)}{\sum_{i=1}^{4} d\left(\boldsymbol{\mu}_i,\boldsymbol{\mu}_3\right)} = 0.4807, \tag{34}$$

and the normalized distance between S_3 and S_4 is:

$$\frac{d\left(\boldsymbol{\mu}_4,\boldsymbol{\mu}_3\right)}{\sum_{i=1}^{4} d\left(\boldsymbol{\mu}_i,\boldsymbol{\mu}_3\right)} = 0.1108, \tag{35}$$

where $d(\bullet)$ is the Euclidean distance. Thus, we set $P(S_{CM}=S_2|S=S_3)=0.1$ and $P(S_{CM}=S_4|S=S_3)=0.2$. The values of the other elements in $P(S_{CM}|S)$ are determined in a similar way and reported in Table 6. Once the integrated estimation of the degradation state is obtained, risk updating and prediction can be performed by (23) and (24), respectively.

Table 5 Values of S, S_{CM} and S_{IN} at different time instants.

	$t=30(d)$	$t=35(d)$	$t=50(d)$
S	S_2	S_3	S_3
S_{CM}	S_2	S_2	S_3
S_{IN}	S_2	S_3	S_2

Table 6 Values of $P(S_{CM}|S)$.

	$S=S_1$	$S=S_2$	$S=S_3$	$S=S_4$
$P(S_{CM}=S_1\|S)$	0.9	0	0	0
$P(S_{CM}=S_2\|S)$	0.05	0.9	0.1	0.1
$P(S_{CM}=S_3\|S)$	0.05	0.1	0.9	0.1
$P(S_{CM}=S_4\|S)$	0	0	0	0.8

6.3 Results and discussion

The results of risk updating and prediction at $t=30,35$ and $50(d)$ are given in Figure 15. In Figure 15, we also show the results from using only condition monitoring data and inspection data, for comparison.

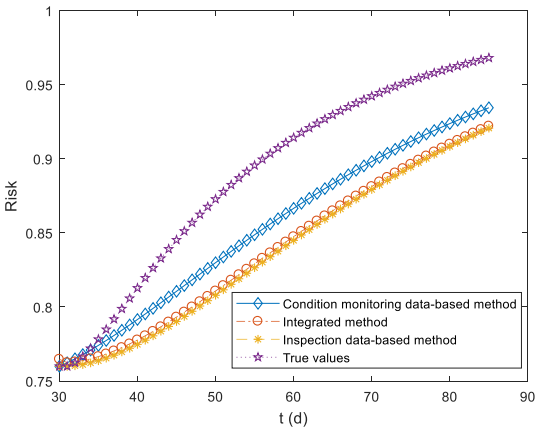

(a) $t = 30(d)$

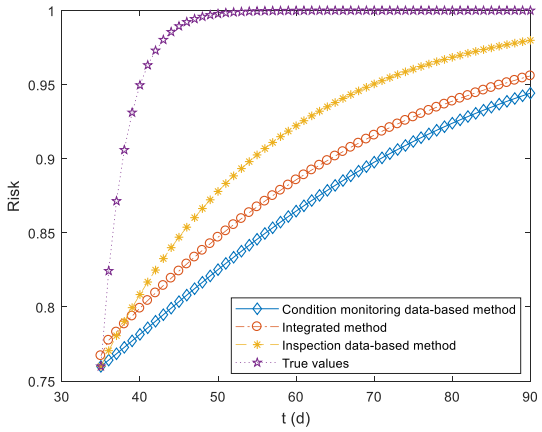

(b) $t = 35(d)$

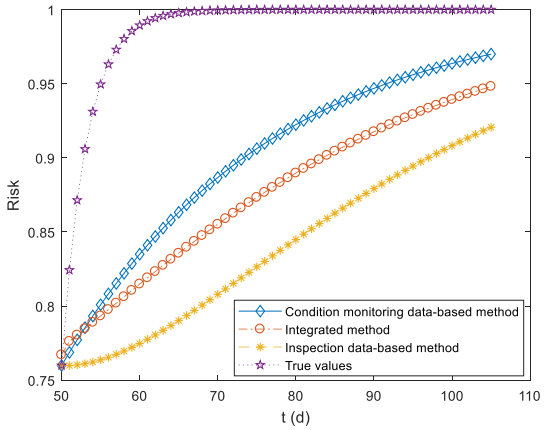

(c) $t = 50(d)$

Figure 15 The results of risk updating and prediction.

As shown in Figure 15(a), at $t = 30(d)$, the results from all the three methods are close to each other. This can be explained from Table 5: at $t = 30(d)$, both data sources correctly identify the true degradation states. However, when compared to the true risk values, the updated and predicted risks from all the three methods show relatively large discrepancies. This discrepancy is mainly due to the estimation errors in the offline step (see (32) and (33)), as we have only four samples in the training data set. A possible way to increase the accuracy of risk updating is, then, to increase the sample size of the training data in the offline step.

It can be seen from Table 5 that at $t = 35(d)$, the inspection data give correct information on the current degradation state while condition monitoring data do not. From Figure 15(b), it can be seen that the developed data-integration method improves the DRA results from the condition monitoring data-based method, as it integrates the correct information from inspection data. On the other hand, when the inspection data fail to give the correct information $(t = 50(d))$, it can be seen from Figure 15(c) that the developed data integration method can also correct the misleading results obtained from using only the inspection data. Hence, in general, applying the

developed data integration method can achieve a more robust DRA result than using the two data sources individually.

In Figure 16, we compare the developed DRA method with the conventional ETA method in [2]. It can be seen from Figure 16 that the results from the developed DRA method are closer to the true risk values than those of the standard ETA. This is because through the integration of inspection and conditon monitoring data, the developed method is able to capture the time-dependent behavior of the recirculation pump resulting from the degradation of the bearing. The standard ETA, however, fails to capture such time-dependencies as it assumes that the event probabilities do not change although the real system/component ages over time.

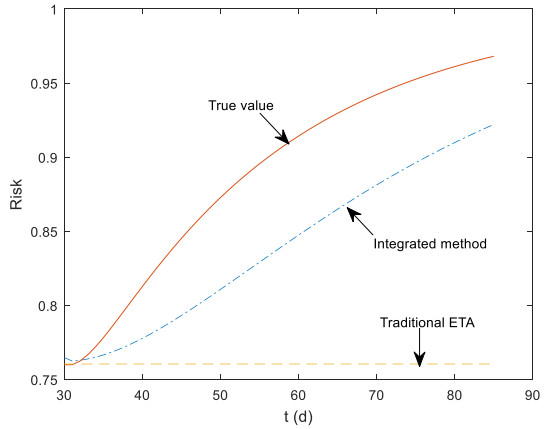

(a) $t = 30(d)$

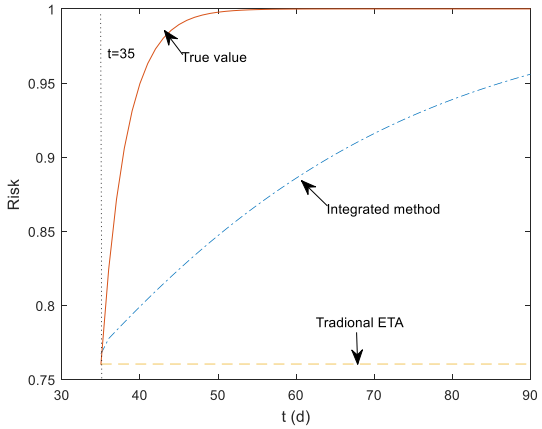

(b) $t = 35(d)$

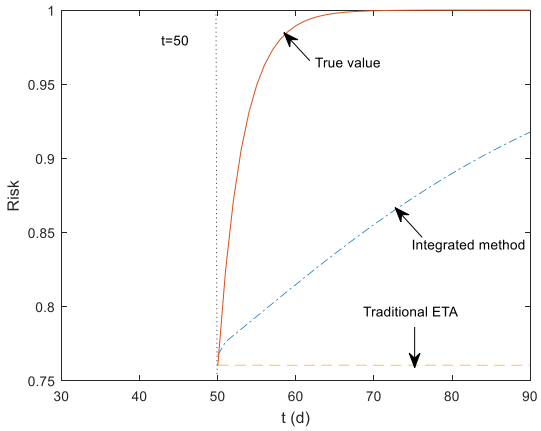

(c) $t = 50(d)$

Figure 16 Comparisons of traditional ETA and DRA.

Additionally, as can be seen from Figure 16, the true risk is higher than the one estimated by the developed method. The inaccuracy of the risk estimation is caused by the imprecise estimation of the parameters in the HM-GMM (equation 32), which is primarily due to the small sample size in the offline training of the HM-GMM (see Figure 4). It can be seen from equations (32) and (33) that, since we have only four samples in the offline training phase, the estimated transition probability differs from its true value. Particularly, the probability of system

remaining in S_3 given that it enters S_3 is estimated to be $a_{33} = 0.9565,$ which is larger than its true value $a_{33} = 0.7150.$ This indicates that the trained HM-GMM trends to overestimate the reliability of the safety barrier (S_4 is the failure state), and, hence, underestimate the risk, in this case. The inaccuracy of the estimation is caused by the fact that we have only four samples from the real dataset, for the offline training phase. In the numerical case study (Section 5), it is shown that with 10^4 training samples, the estimation accuracy is satisfactory.

A major issue with the EM algorithm (Algorithm 1) is that, when the sample size is small, there can be large uncertainty on the estimated parameter values. This uncertainty, if not properly addressed, might greatly impact the estimation accuracy of the reliability of the safety barriers, and, then, the calculated risk. One way to capture the uncertainty in the estimated risk caused by parameter estimation is to conduct a bounding risk analysis by using Bayesian inference [20, 46, 47], where posterior distributions of the parameters, rather than point estimators, are calculated to represent the parametric uncertainty. The uncertainty in the parameter estimation can be represented in terms of the credible intervals. By propagating the parametric uncertainty, a credibility interval can also be obtained for the estimated risk, which can help the decision-makers understand the confidence on the risk estimations.

7. Conclusions

In this paper, a framework has been presented to integrate condition monitoring data and inspection data for DRA. A HM-GMM has been developed to estimate the degradation states of the safety barriers based on the condition monitoring data. The estimated degradation states are integrated with the inspection data for DRA by a BN model. A numerical case study and a real-word application on a NPP accident risk assessment model (an ET) have been conducted. The results show that, as expected, integrating the two data sources into the DRA gives more accurate and robust results than using any one of the two individual data sources.

There are some challenges to be addressed when applying the developed model to real-life large-scale systems (of systems). The first one is that, to ensure the accuracy of the developed method, a sufficient number of training samples is needed. This might not be the case for real-world systems. To address this challenge, the estimation of the values of the parameters of the HM-GMM can be embedded within a Bayesian inference framework for a bounding analysis that gives due account to uncertainties. Other future developments should consider the extension of the developed model to systems with multiple degrading components and repairable components.

The current method only considers a discrete time discrete state Markov model as the degradation model. A future work is to extend the developed framework to other degradation models, e.g. the Brownian motion model

[48], Gamma process model [49], etc. Moreover, in the current framework, the parameters of HM-GMM are estimated offline; in the future, online updating of the parameters can be considered in order to improve the accuracy of the DRA.

References

[1] Yang, X., S. Haugen, and N. Paltrinieri, *Clarifying the concept of operational risk assessment in the oil and gas industry.* Safety Science, 2017.

[2] Huang, D., T. Chen, and M.-J.J. Wang, *A fuzzy set approach for event tree analysis.* Fuzzy sets and systems, 2001. **118**(1): p. 153-165.

[3] Compare, M., et al., *Semi-Markov model for the oxidation degradation mechanism in gas turbine nozzles.* IEEE Transactions on Reliability, 2016. **65**(2): p. 574-581.

[4] Chiachío, J., et al., *Condition-based prediction of time-dependent reliability in composites.* Reliability Engineering & System Safety, 2015. **142**: p. 134-147.

[5] Kim, H., et al., *Reliability data update using condition monitoring and prognostics in probabilistic safety assessment.* Nuclear Engineering and Technology, 2015. **47**(2): p. 204-211.

[6] Di Maio, F., F. Antonello, and E. Zio, *Condition-based probabilistic safety assessment of a spontaneous steam generator tube rupture accident scenario.* Nuclear Engineering and Design, 2018. **326**: p. 41-54.

[7] Zhao, X., X. Guo, and X. Wang, *Reliability and maintenance policies for a two-stage shock model with self-healing mechanism.* Reliability Engineering & System Safety, 2018. **172**: p. 185-194.

[8] Sklet, S., *Safety barriers: Definition, classification, and performance.* Journal of Loss Prevention in the Process Industries, 2006. **19**(5): p. 494-506.

[9] Landucci, G., et al., *Quantitative assessment of safety barrier performance in the prevention of domino scenarios triggered by fire.* Reliability Engineering & System Safety, 2015. **143**: p. 30-43.

[10] Kim, H., J.T. Kim, and G. Heo, *Failure rate updates using condition-based prognostics in probabilistic safety assessments.* Reliability Engineering & System Safety, 2018. **175**: p. 225-233.

[11] Villa, V., et al., *Towards dynamic risk analysis: a review of the risk assessment approach and its limitations in the chemical process industry.* Safety science, 2016. **89**: p. 77-93.

[12] Paltrinieri, N., et al., *Dynamic approach to risk management: application to the Hoeganaes metal dust accidents.* Process Safety and Environmental Protection, 2014. **92**(6): p. 669-679.

[13] Abimbola, M., F. Khan, and N. Khakzad, *Dynamic safety risk analysis of offshore drilling.* Journal of Loss Prevention in the Process Industries, 2014. **30**: p. 74-85.

[14] Khakzad, N., F. Khan, and N. Paltrinieri, *On the application of near accident data to risk analysis of major accidents.* Reliability Engineering & System Safety, 2014. **126**: p. 116-125.

[15] Yang, M., F.I. Khan, and L. Lye, *Precursor-based hierarchical Bayesian approach for rare event frequency estimation: a case of oil spill accidents.* Process safety and environmental protection, 2013. **91**(5): p. 333-342.

[16] Wang, H., et al., *Dynamic quantitative operational risk assessment of chemical processes.* Chemical Engineering Science, 2016. **142**: p. 62-78.

[17] Hashemi, S.J., S. Ahmed, and F. Khan, *Loss functions and their applications in process safety assessment.* Process Safety Progress, 2014. **33**(3): p. 285-291.

[18] Zarei, E., et al., *Dynamic safety assessment of natural gas stations using Bayesian network.* Journal of hazardous materials, 2017. **321**: p. 830-840.

[19] Adedigba, S.A., et al., *Data-driven dynamic risk analysis of offshore drilling operations.* Journal of Petroleum Science and Engineering, 2018. **165**: p. 444-452.

[20] Zeng, Z. and E. Zio, *Dynamic Risk Assessment Based on Statistical Failure Data and Condition-Monitoring Degradation Data.* IEEE Transactions on Reliability, 2018. **67**(2): p. 609-622.

[21] Kalantarnia, M., F. Khan, and K. Hawboldt, *Dynamic risk assessment using failure assessment and Bayesian theory.* Journal of Loss Prevention in the Process Industries, 2009. **22**(5): p. 600-606.

[22] Meel, A. and W.D. Seider, *Plant-specific dynamic failure assessment using Bayesian theory.* Chemical Engineering Science, 2006. **61**(21): p. 7036-7056.

[23] Meel, A., et al., *Operational risk assessment of chemical industries by exploiting accident databases.* Journal of Loss Prevention in the Process Industries, 2007. **20**(2): p. 113-127.

[24] Khakzad, N., F. Khan, and P. Amyotte, *Dynamic risk analysis using bow-tie approach.* Reliability Engineering & System Safety, 2012. **104**: p. 36-44.

[25] Shalev, D.M. and J. Tiran, *Condition-based fault tree analysis (CBFTA): A new method for improved fault tree analysis (FTA), reliability and safety calculations.* Reliability Engineering & System Safety, 2007. **92**(9): p. 1231-1241.

[26] Aizpurua, J.I., et al., *Improved dynamic dependability assessment through integration with prognostics.* IEEE

Transactions on Reliability, 2017. **66**(3): p. 893-913.
[27] Zadakbar, O., F. Khan, and S. Imtiaz, *Dynamic Risk Assessment of a Nonlinear Non‐Gaussian System Using a Particle Filter and Detailed Consequence Analysis.* The Canadian Journal of Chemical Engineering, 2015. **93**(7): p. 1201-1211.
[28] Liu, J. and E. Zio, *System dynamic reliability assessment and failure prognostics.* Reliability Engineering & System Safety, 2017. **160**: p. 21-36.
[29] Nguyen, H.-P., J. Liu, and E. Zio, *Dynamic-weighted ensemble for fatigue crack degradation state prediction.* Engineering Fracture Mechanics, 2018. **194**: p. 212-223.
[30] Liu, Y., et al., *Bayesian reliability and performance assessment for multi-state systems.* IEEE Transactions on Reliability, 2015. **64**(1): p. 394-409.
[31] Liu, Y. and C.-J. Chen, *Dynamic reliability assessment for nonrepairable multistate systems by aggregating multilevel imperfect inspection data.* IEEE Transactions on Reliability, 2017. **66**(2): p. 281-297.
[32] Nielsen, J.S. and J.D. Sørensen, *Bayesian Estimation of Remaining Useful Life for Wind Turbine Blades.* Energies, 2017. **10**(5): p. 664.
[33] Lees, F., *Lees' Loss prevention in the process industries: Hazard identification, assessment and control*. 2012: Butterworth-Heinemann.
[34] Tobon-Mejia, D.A., et al., *A data-driven failure prognostics method based on mixture of Gaussians hidden Markov models.* IEEE Transactions on Reliability, 2012. **61**(2): p. 491-503.
[35] Soualhi, A., et al., *Prognosis of bearing failures using hidden Markov models and the adaptive neuro-fuzzy inference system.* IEEE Transactions on Industrial Electronics, 2014. **61**(6): p. 2864-2874.
[36] Shahraki, A.F., O.P. Yadav, and H. Liao, *A Review on Degradation Modelling and Its Engineering Applications.* International Journal of Performability Engineering, 2017. **13**(3): p. 299.
[37] Alizadeh, S. and S. Sriramula, *Unavailability assessment of redundant safety instrumented systems subject to process demand.* Reliability Engineering & System Safety, 2018. **171**: p. 18-33.
[38] Jiang, H., J. Chen, and G. Dong, *Hidden Markov model and nuisance attribute projection based bearing performance degradation assessment.* Mechanical Systems and Signal Processing, 2016. **72-73**: p. 184-205.
[39] Javed, K., et al., *Enabling health monitoring approach based on vibration data for accurate prognostics.* IEEE Transactions on Industrial Electronics, 2015. **62**(1): p. 647-656.
[40] Rabiner, L.R., *A tutorial on hidden Markov models and selected applications in speech recognition.* Proceedings of the IEEE, 1989. **77**(2): p. 257-286.
[41] Le, T.T., F. Chatelain, and C. Bérenguer, *Multi-branch hidden Markov models for remaining useful life estimation of systems under multiple deterioration modes.* Proceedings of the Institution of Mechanical Engineers, Part O: Journal of Risk and Reliability, 2016. **230**(5): p. 473-484.
[42] Tsai, C.W., N.-K. Wu, and C.-H. Huang, *A multiple-state discrete-time Markov chain model for estimating suspended sediment concentrations in open channel flow.* Applied Mathematical Modelling, 2016. **40**(23): p. 10002-10019.
[43] Yang, S.H., et al., *Performance evaluation of an advanced integral reactor against an anticipated transient without scram.* Annals of Nuclear Energy, 2006. **33**(8): p. 655-663.
[44] Baraldi, P. and E. Zio, *A combined Monte Carlo and possibilistic approach to uncertainty propagation in event tree analysis.* Risk Analysis, 2008. **28**(5): p. 1309-1326.
[45] NASA, *Prognostic Data Repository: Bearing Data Set NSF I/UCRC Center for Intelligent Maintenance Systems*, 2010.
[46] Zhang, D., A.D. Bailey, and D. Djurdjanovic, *Bayesian identification of hidden markov models and their use for condition-based monitoring.* IEEE Transactions on Reliability, 2016. **65**(3): p. 1471-1482.
[47] Fan, M., et al., *A Sequential Bayesian Approach for Remaining Useful Life Prediction of Dependent Competing Failure Processes.* IEEE Transactions on Reliability, 2018. **68**(1): p. 317-329.
[48] Zhai, Q. and Z.-S. Ye, *RUL prediction of deteriorating products using an adaptive Wiener process model.* IEEE Transactions on Industrial Informatics, 2017. **13**(6): p. 2911-2921.
[49] Zhai, Q. and Z.-S. Ye, *Robust degradation analysis with non-Gaussian measurement errors.* IEEE Transactions on Instrumentation and Measurement, 2017. **66**(11): p. 2803-2812.